NANO LETTERS

Letter

pubs.acs.org/NanoLett

Can Two-Dimensional Boron Superconduct?

Evgeni S. Penev, Alex Kutana, and Boris I. Yakobson*

Department of Materials Science and NanoEngineering, Rice University, Houston, Texas 77005, United States

Supporting Information

ABSTRACT: Two-dimensional boron is expected to exhibit various structural polymorphs, all being metallic. Additionally, its small atomic mass suggests strong electron−phonon coupling, which in turn can enable superconducting behavior. Here we perform first-principles analysis of electronic structure, phonon spectra, and electron−phonon coupling of selected 2D boron polymorphs and show that the most stable structures predicted to feasibly form on a metal substrate should also exhibit intrinsic phonon-mediated superconductivity, with estimated critical temperature in the range of $T_c \approx 10-20$ K.

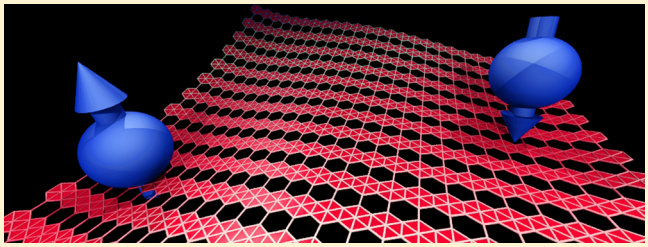

KEYWORDS: *Two-dimensional boron, conventional superconductivity, electron−phonon coupling, first-principles calculations*

Carbon, boron, and nitrogen have been the core components of a plethora of low-dimensional materials that rekindled both fundamental and applied research over the past decade. Two-dimensional (2D) compounds in the C−B−N ternary phase diagram are abundant.[1] However, only carbon is known to exist as a stable, single-layer, 2D *elemental* material, graphene. Elemental nitrogen is a diatomic gas, whereas boron exhibits various bulk 3D polymorphs.[2] The question of whether elemental B can exist in a 2D conformation[3] has motivated both theoretical and experimental search for this elusive material.

Theoretically, we have previously demonstrated[4] that flat, free-standing single-layer B would exhibit rich polymorphism with multiple, all metallic, low-energy structures in the range of compositions $x \simeq 0.1-0.15$ of the pseudoalloy $B_{1-x}V_x$, V being a vacancy in the underlying triangular B lattice. This picture does not change qualitatively when considering 2D B on selected metals, proposed as plausible candidate substrates to use in experimental synthesis via chemical vapor deposition (CVD).[5,6] However, the metal substrate does (i) shift the lowest-energy polymorphs to slightly higher x, and (ii) "magnify" the energy separation between the configurations at the same x. Thus, it appears that atomically thin layer of boron can combine *lightweight* and *metallicity* in a novel 2D material. In fact, the honeycomb B sublattice ($x = 1/3$) and its two-dimensionality are the root of superconductivity in MgB_2.[7−9] Moreover, the essential physics of the basic high-T_c cuprates is ultimately contained within the 2D copper−oxygen planes.[10] An intriguing question then arises as to whether free-standing 2D B can be superconducting.

Here, we perform first-principles density functional theory (DFT) calculations of the electron−phonon coupling strength[11] λ in several polymorphs of 2D B to estimate the superconducting critical temperature T_c and show that 2D boron may indeed be a conventional superconductor. The free-energy convex hull of $B_{1-x}V_x$ features multiple polymorphs[4,6] whose detailed exploration is impractical. Instead, a few specific polymorphs are selected based on simple energy preference arguments and computational feasibility. The 2D B polymorphs can formally be considered as alloys of the two limit compositions: the triangular $B_{\triangle}$ lattice ($x = 0$)[3,12,13] and the honeycomb $B_{\hexagon}$ lattice ($x = 1/3$). While functionalization/doping is an inopportune prerequisite for emergence of metallicity and conventional superconductivity in 2D materials like graphene and its derivatives[14−17] as well as black phosphorus,[18] all $B_{1-x}V_x$ configurations are metallic. However, adding vacancies to $B_{\triangle}$ (creating hexagonal voids), or B atoms to $B_{\hexagon}$ (filling in the hexagonal voids) is essentially a "self-doping" process[19,20] that can rationalize the overall energy stabilization trends. We thus consider the limiting case of the $B_{\triangle}$ lattice ($p2mm$ symmetry, with diatomic basis, Figure 1,

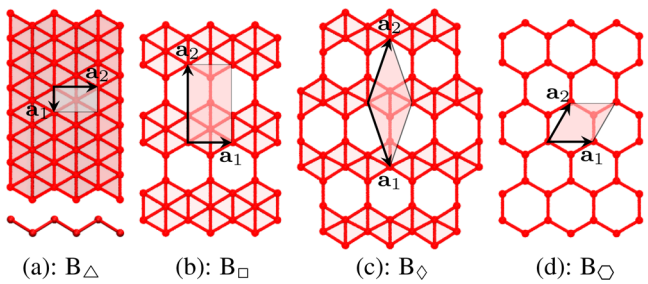

Figure 1. Atomic structure of selected 2D B polymorphs with the unit cells and the lattice vectors $\mathbf{a}_{1,2}$ indicated. (a) Limit case of a buckled triangular $B_{\triangle}$ layer, $x = 0$; side view along $\mathbf{a}_1$ is shown in the lower image. (b) The lowest-energy structure for $x = 1/6$, $B_{\square}$. (c) 2D B layer with $x = 1/5$, denoted as $B_{\diamondsuit}$. (d) The boron isomorph of graphene, $B_{\hexagon}$, $x = 1/3$.

Received: January 6, 2016
Revised: March 8, 2016
Published: March 22, 2016

DOI: 10.1021/acs.nanolett.6b00070
Nano Lett. 2016, 16, 2522−2526

panel a), the lowest-energy structure at $x = 1/6$ (both as free-standing sheet,[4] as well as on the Ag(111) surface[6]), $B_{\square}$, shown in Figure 1, panel b, and also one at slightly higher vacancy fraction, $x = 1/5$, $B_{\diamondsuit}$, shown in Figure 1, panel c. The latter is sometimes referred to as "χ_3", has the smallest unit cell, and is one of the most stable sheets with coordination numbers four and five.[21] The honeycomb limit in Figure 1, panel d is not included, as it is too high in energy,[4] and also displays significant lattice instability.

Our calculations are based on the microscopic theory of Bardeen, Cooper, and Schrieffer (BSC),[22] as generalized by Migdal[23] and Eliashberg.[24] Critical temperatures T_c are estimated using the modified approximate McMillan equation,[25] $k_B T_c = (\hbar\omega_{ln}/1.2)\exp[-1.02(1+\lambda)/(\lambda-\mu^*-0.62\mu^*\lambda)]$, where the ω_{ln} prefactor is a properly defined logarithmic average frequency suggested by Allen and Dynes,[26] and μ^* is a parameter, typically ∼0.1, accounting for the effective Coulomb repulsion.[27,28] The computational protocol, as implemented in the QUANTUM ESPRESSO package,[29] is well established and has been applied to various other 2D systems;[14,15,17,18] more details are given in the Supporting Information. The electronic spectra $\varepsilon_{\mathbf{k}}$, phonon dispersions $\omega_{\mathbf{q}\nu}$, and electron−phonon coupling parameters λ for the $B_{\triangle}$, $B_{\square}$, and $B_{\diamondsuit}$ structures were calculated within the local-density approximation using plane-wave basis set (energy cutoff of 70 Ry) and norm-conserving pseudopotential. The choice of electron momentum $\mathbf{k}$ and phonon wavevector $\mathbf{q}$-grids is based on a set of benchmarks for each separate B lattice to ensure converged T_c. Gaussian smearing of 0.02 Ry width was used for integration over the 2D Fermi contour in calculating the electron−phonon coupling coefficients $\lambda_{\mathbf{q}\nu}$, for determining the Fermi level ε_F, the corresponding total electronic density of states $N(\varepsilon_F)$, and to calculate the isotropic Eliashberg spectral function $\alpha^2F(\omega)$. In all cases below, the T_c values are reported using $\mu^* = 0.1$ in the McMillan equation. Since there is no reliable way to determine this parameter within the present computational scheme, we only assess its effect on T_c by varying its value in certain range (see Supporting Information).

Buckled Triangular $B_{\triangle}$ Lattice. The close-packed, flat $B_{\triangle}$ sheet is known to be higher in energy, $\gtrsim 0.3$ eV/atom,[4] above the ground-state region around $x \approx 1/8$. Formation of a buckled zigzag pattern[12,13] (nearly doubled lattice periodicity along $\mathbf{a}_2$), Figure 1, panel a, can lower its energy by ∼0.2 eV/atom.[4,19] Such lattice anisotropy leads to largely dispersive bands crossing the Fermi level along Γ−X and Γ−M, but not along Γ−Y, corresponding to the "soft" direction perpendicular to the up/down atomic ridges, Figure 2, panel a. Importantly, the Fermi contour,[13] shown in Figure 2, panel b, comprises segments of two bands of different, π- and σ-character with similar, low $N_l(\varepsilon_F)$. Its p_z-derived branch (forming essentially width-modulated electron strip along Γ−Y) has a pair of parallel sections corresponding to perfect nesting along Γ−X with $\mathbf{Q} = (1/4,0)$. Note that the p_z-band topology, inset in Figure 2, panel a, is such that the nesting will be preserved in a weak electron or hole doping rigid-band scenario. The p-bands are degenerate along Y−M resulting in a set of discrete "Fermi points" at the BZ boundary where the Fermi contour segments intersect at 90°. The tangents (dotted lines in Figure 2, panel b) extending from these points form a 45°-rotated square, centered at Y, with the other two corners located at the Γ point.

The Fermi contour nesting may be identifiable also in the phonon spectrum of the $B_{\triangle}$ lattice, Figure 3: a sharp phonon softening/dip is found for one of the branches at $\mathbf{q}_1 = \mathbf{Q}$ along

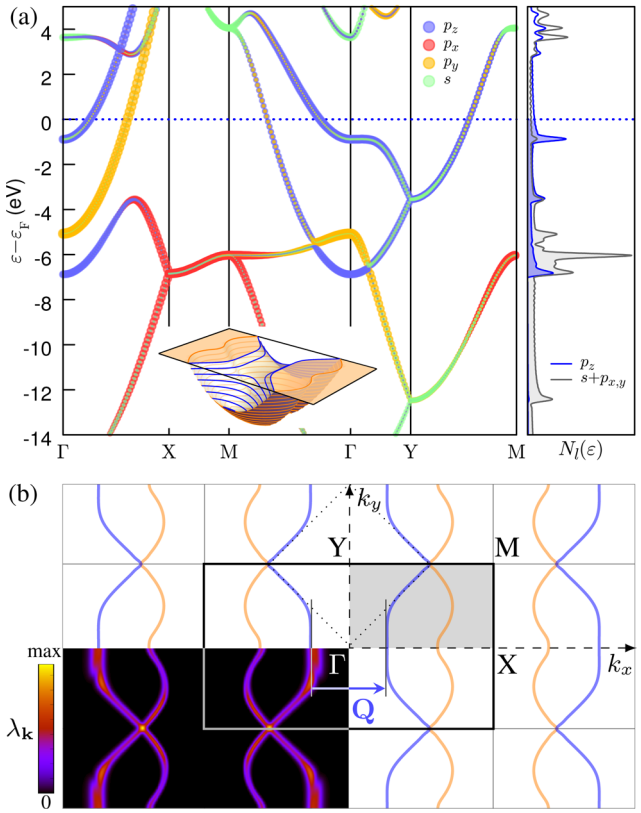

Figure 2. (a) Band structure of the $B_{\triangle}$ sheet, and the corresponding projected density of states (right panel). The orbital character of the bands is thickness and color encoded. The complete energy surfaces of the two conduction bands, clipped at ε_F, are shown in the inset. (b) Fermi contour of $B_{\triangle}$ in the extended Brillouin zone (BZ) scheme (the conventional BZ is shown as bold rectangle, with its irreducible part shaded). The separate Fermi contour segments are colored according to their band origin. The lower left quarter shows the magnitude of the effective $\mathbf{k}$-resolved electron−phonon coupling $\lambda_{\mathbf{k}}$.

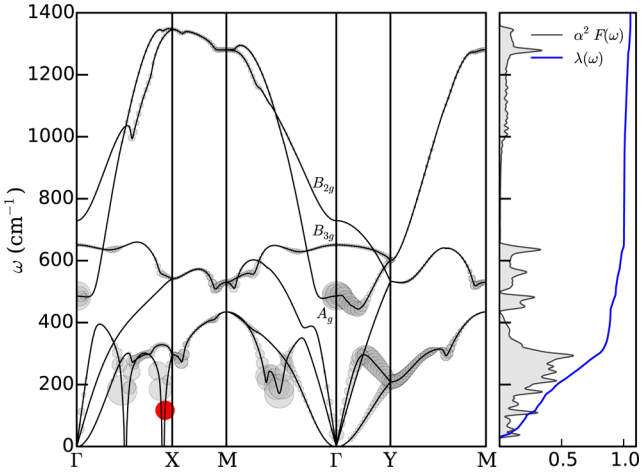

Figure 3. Phonon spectrum and electron−phonon coupling of the $B_{\triangle}$ sheet. The area of the circles is proportional to the magnitude of electron−phonon couplings $\lambda_{\mathbf{q}\nu}$. The area of the red circle has been reduced 10-fold. Symmetries of the modes with large couplings at Γ are also given. The right panel shows the calculated Eliashberg spectral function $\alpha^2F(\omega)$ and $\lambda(\omega)$.

Γ−X. A second Kohn anomaly[30] exists at $\mathbf{q}_2 = (0.453,0)$ (essentially a single $\mathbf{q}$-point of the 128 × 64 grid), in close

DOI: 10.1021/acs.nanolett.6b00070
Nano Lett. 2016, 16, 2522−2526

proximity to the X point, with the phonon frequency becoming imaginary. The norm and direction of the $\mathbf{q}_2$-vector appear close to the nesting between p_y and p_z contours along Γ−X, Figure 2, panel b, although much less pronounced, suggesting a structural instability.

These two regions in the phonon BZ are characterized by very large coupling $\lambda_{\mathbf{q}\nu}$, with those at $\mathbf{q}_2$ (red circle in Figure 3) being nearly an order of magnitude larger than for any other $(\mathbf{q},\nu)$. The spectral weight is rather unevenly distributed over the frequency range (80% of the total coupling is determined by ∼20% of the spectrum, $\omega < 300$ cm^{-1}), with the major contribution, as seen from the calculated α^2F, coming from the phonon branches with $\omega_{\mathbf{q}\nu} \simeq 200-300$ cm^{-1}. The total isotropic electron−phonon coupling $\lambda = 2\int_0^\infty d\omega\alpha^2F(\omega)\omega^{-1}$ is found to be $\lambda \simeq 1.1$, rendering the $B_{\triangle}$ sheet an intermediate-coupling conventional superconductor with $T_c \simeq 21$ K. As these soft modes and couplings may change significantly after small structural rearrangements, it is necessary to examine possible effect of such perturbations on the T_c. We first note that these soft modes are localized in a rather narrow region of the BZ and are expected to have small contribution to the total electron−phonon coupling. Omitting *all* couplings with $\omega < 100$ cm^{-1} yields $T_c \simeq 14$ K for the $B_{\triangle}$ structure, suggesting more robust superconducting behavior.

Since the Fermi contour, however, originates from two bands of different character similar to MgB_2,[31] it is interesting to explore their relative contribution to a possible superconducting behavior. The contribution is reflected in the effective momentum-dependent coupling $\lambda_{\mathbf{k}}$ (see Supporting Information) for an initial electronic momentum $\mathbf{k}$ scattered to $\mathbf{k}' = \mathbf{k} - \mathbf{q}$ by all possible phonons $\mathbf{q}$, with both initial and final states on the Fermi contour. This quantity is plotted in Figure 2, panel b. Clearly, $\lambda_{\mathbf{k}}$ is peaked at the two points where the π and σ bands are degenerate, but its magnitude is similar along both segments around these cross-points. Relatively large $\lambda_{\mathbf{k}}$ values are also calculated along the nested sections of the p_z-derived segment, but overall no sharp difference is observed between the effective couplings over the two segments of the Fermi contour.

Flat $B_{\square}$ Sheet. The $B_{\square}$ polymorph, Figure 1, panel b, features stripes of filled and empty hexagons along the zigzag direction resulting in *p2mm* symmetry. This is the lowest energy structure with stoichiometry $x = 1/6$ for both the free-standing sheet[4] and on a Ag(111) substrate.[6] Unlike $B_{\triangle}$, the relaxed $B_{\square}$ geometry is truly planar. However, its flexural acoustic mode has imaginary frequencies near the Γ point, pointing to lattice instabilities corresponding to long-wave undulations. In two-dimensional membranes, and particularly in graphene, flexural phonons near $\mathbf{q} = 0$ are the source of crumpling instability at any finite temperature.[32,33] The imaginary frequencies near the Γ point were eliminated altogether by applying a uniform tensile strain as small as 1% (see Supporting Information), with no observable effect on the electronic structure. The band structure of the striped $B_{\square}$, Figure 4, panel a, shows ∼3.5 eV gap separating the bonding σ and antibonding σ^* states. Nearly all σ states are filled and remaining electrons partially fill the p_z-derived π states. As a result, the Fermi contour consists of two $p_{x,y}$-derived small hole pockets around Γ, and p_z-derived large ellipsoidal electron pocket centered at Y, and a narrow width-modulated strip along X−M, Figure 4, panel b. A noticeable feature is that the three bands simultaneously cross at ε_F, and all Fermi contour segments touch on the Γ−Y line, in proximity to the BZ center.

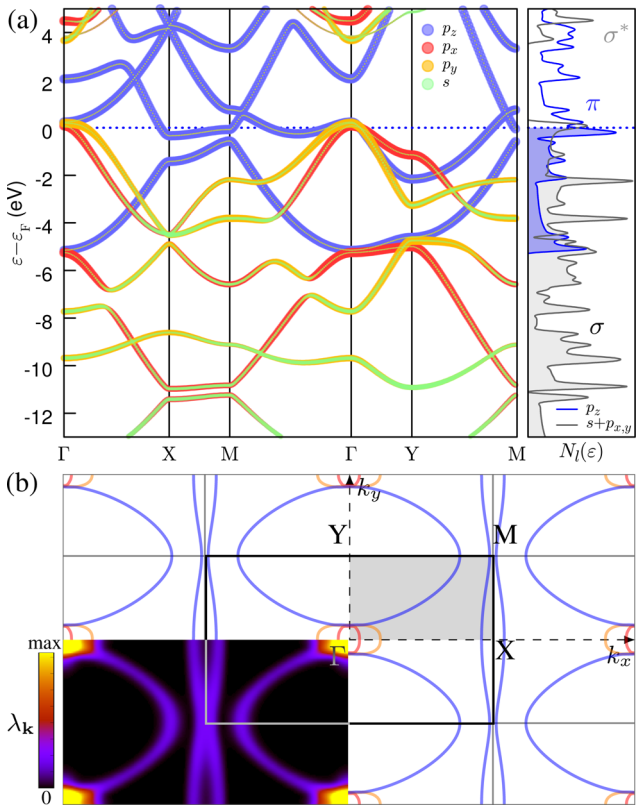

Figure 4. (a) Band structure of the $B_{\square}$ sheet, and the corresponding projected density of states (right panel). The orbital character of the bands is thickness and color encoded. (b) Fermi contour and effective electron−phonon coupling $\lambda_{\mathbf{k}}$, similar to Figure 2, panel b.

As seen from the $\lambda_{\mathbf{k}}$ color map in Figure 4, panel b, the electron−phonon interaction is considerably anisotropic with largest values localized on the three segments around Γ, while $\lambda_{\mathbf{k}}$ is relatively small and varies little on remaining length of the π-contours.

The phonon spectrum of the "stabilized" $B_{\square}$ sheet is shown in Figure 5. Indeed, the phonon dispersion for the flexural mode becomes linear near the Γ point as a result of strain.[33]

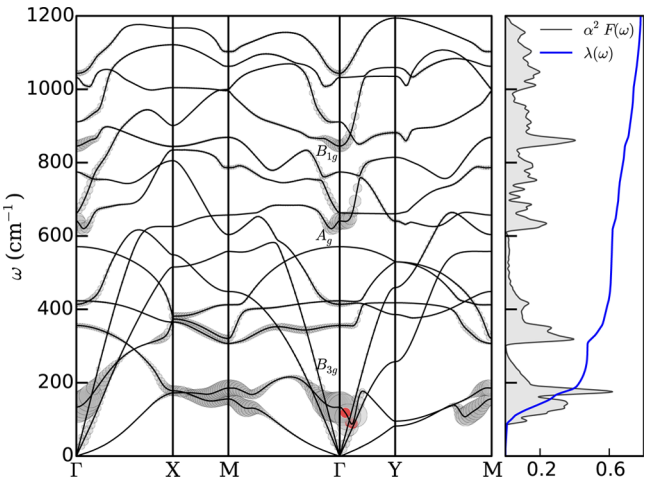

Figure 5. Phonon dispersions, electron−phonon coupling, Eliashberg spectral function, and cumulative frequency-dependent coupling $\lambda(\omega)$ of the $B_{\square}$ structure under 1% uniform tensile strain. The circles show electron−phonon couplings $\lambda_{\mathbf{q}\nu}$, similar to Figure 3.

DOI: 10.1021/acs.nanolett.6b00070
Nano Lett. 2016, 16, 2522−2526

The calculated total electron−phonon coupling parameter is $\lambda \simeq 0.8$ and results in $T_c = 16$ K. About half of λ is due to coupling to low-frequency phonons $\omega_{q\nu} \lesssim 200$ cm^{-1}, especially the out of plane mode B_{3g} with "rocking" type up/down atomic displacements. However, we find ≃20% contribution also from higher frequency optical branches, mostly due to the A_g and B_{1g} in-plane modes with $\omega > 600$ cm^{-1}.

Flat $B_{\diamondsuit}$ Sheet. This is a planar polymorph of slightly higher vacancy fraction $x = 0.2$ and maximum atomic coordination number of 5. The neighboring vacancy rows, compared to those in $B_{\square}$, are shifted by half of the lattice constant in the zigzag direction, thus resulting in a planar *c2mm* symmetry, Figure 1, panel c. Similar to $B_{\square}$, the $B_{\diamondsuit}$ has small imaginary phonon frequencies near the Γ point that can be eliminated by applying 1% uniform tensile strain, which is small enough for any effect on the band structure to be observed. The total $N(\varepsilon_F)$ is dominated by the p_z-derived band, but the presence of both π and σ bands results in a complex multisegment Fermi contour, Figure 6, panel b. It is interesting to note that in this case λ_k is considerably larger on the wavy σ segments along Γ−Y.

The phonon spectrum of the slightly strained $B_{\diamondsuit}$ is shown in Figure 7. The spectrum displays a Kohn anomaly as a sharp dip along the X′−Y line with the phonon frequency at that **q** becoming imaginary. However, this feature is of different nature than the instability at the Γ point, both because of its shape and the fact that it generally occurs at an incommensurate **q**-vector. It is also clear that the origin of this instability is similar to that of the two instabilities along Γ−X in $B_{\triangle}$, Figure 3. The spectral weight is distributed over the entire frequency range, and the calculated total $\lambda \simeq 0.6$ of this sheet is in the weak-coupling regime, with an estimated $T_c = 12$ K.

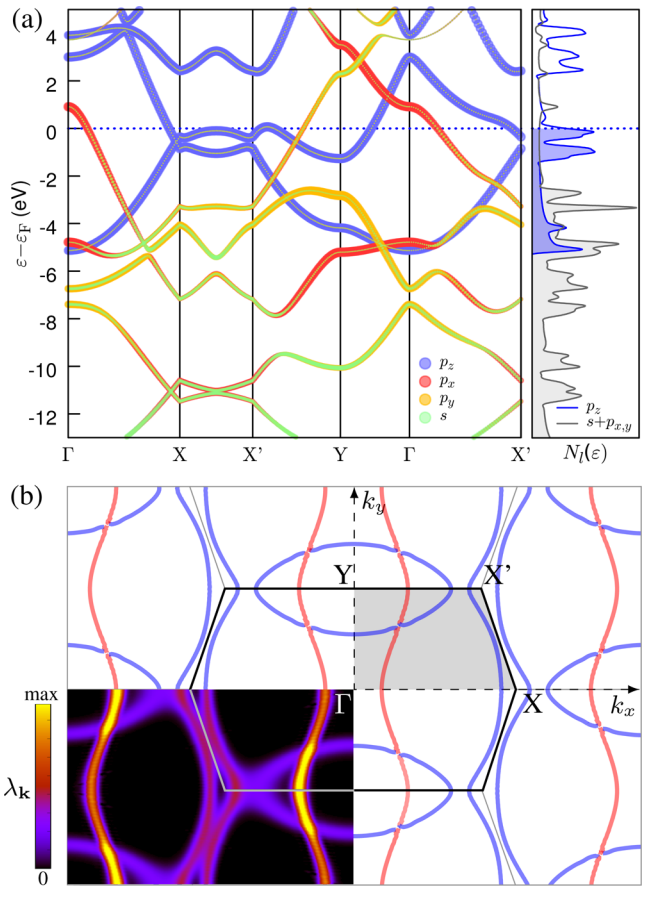

Figure 6. (a) Band structure of the $B_{\diamondsuit}$ sheet, and the corresponding projected density of states (right panel). The orbital character of the bands is thickness and color encoded. (b) Fermi contour and effective electron−phonon coupling λ_k, similar to Figure 2, panel b.

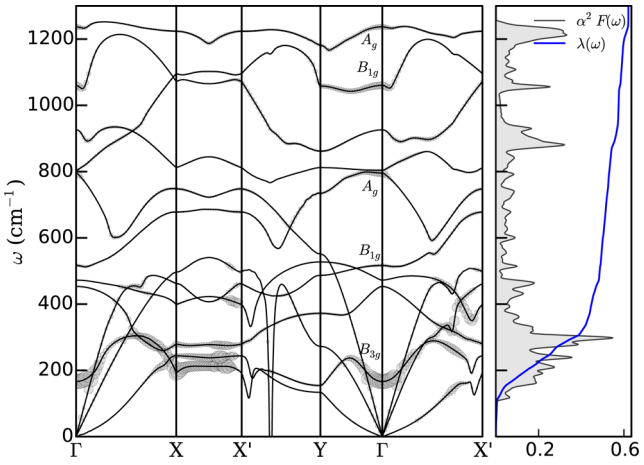

Figure 7. Phonon spectrum, electron−phonon coupling $\lambda_{q\nu}$, Eliashberg spectral function α^2F, and the cumulative frequency-dependent coupling $\lambda(\omega)$ of the $B_{\diamondsuit}$ structure under 1% uniform tensile strain, similar to Figure 3.

In summary, first-principles calculations of the electron−phonon coupling in selected $B_{1-x}V_x$ polymorphs of 2D boron suggest possible intrinsic conventional superconductivity with critical temperatures $T_c \approx 10-20$ K, where T_c increases with decreasing x. All structural models display phonon instabilities as (i) imaginary frequencies near the Γ point and/or (ii) sharp singularities at some general **q** in the phonon BZ. Since 2D boron may form via some deposition growth process on a suitable metal substrate, then such supported polymorphs would be naturally stabilized, but stronger adhesion, for instance, may eventually reduce T_c. It is plausible, however, that 2D boron is "stabilized" by an inert protecting layer such as 2D hexagonal BN, in which case superconducting behavior may well be preserved. Interestingly, during the completion of this manuscript, in a remarkable development, the synthesis of a few 2D B polymorphs on Ag(111) was reported nearly simultaneously by three groups[34−36] landing unequivocal support for our theoretically proposed synthesis routes.[5,6] Additionally, after submission of our manuscript, we became aware of a work discussing possible superconductivity in other, thicker boron films.[37] The present analysis thus should provide valuable insight into the 2D-limit of this fundamental collective phenomenon in elemental boron.[38]

■ ASSOCIATED CONTENT

Supporting Information

The Supporting Information is available free of charge on the ACS Publications website at DOI: 10.1021/acs.nanolett.6b00070.

Methodology, convergence tests, and other computational details (PDF)

■ AUTHOR INFORMATION

Corresponding Author

*E-mail: biy@rice.edu.

DOI: 10.1021/acs.nanolett.6b00070
Nano Lett. 2016, 16, 2522−2526

Author Contributions

‡E.S.P. and A.K. contributed equally to this work.

Notes

The authors declare no competing financial interest.

■ ACKNOWLEDGMENTS

This work was supported by the Office of Naval Research grant N00014-15-1-2372 and, in the structural search analysis part, by the Department of Energy BES grant DE-SC0012547. This research used resources of the National Energy Research Scientific Computing Center (NERSC), supported by the DOE Office of Science under Contract No. DE-AC02-05CH11231, and resources provided by the ERDC DoD Supercomputing Resource Center.

■ REFERENCES

(1) Shi, Z.; Kutana, A.; Yakobson, B. I. *J. Phys. Chem. Lett.* **2015**, *6*, 106−112.
(2) Albert, B.; Hillebrecht, H. *Angew. Chem., Int. Ed.* **2009**, *48*, 8640−8668.
(3) Boustani, I. *Surf. Sci.* **1997**, *370*, 355−363.
(4) Penev, E. S.; Bhowmick, S.; Sadrzadeh, A.; Yakobson, B. I. *Nano Lett.* **2012**, *12*, 2441−2445.
(5) Liu, Y.; Penev, E. S.; Yakobson, B. I. *Angew. Chem., Int. Ed.* **2013**, *52*, 3156−3159.
(6) Zhang, Z.; Yang, Y.; Gao, G.; Yakobson, B. I. *Angew. Chem., Int. Ed.* **2015**, *54*, 13022−13026.
(7) An, J. M.; Pickett, W. E. *Phys. Rev. Lett.* **2001**, *86*, 4366−4369.
(8) Kortus, J.; Mazin, I. I.; Belashchenko, K. D.; Antropov, V. P.; Boyer, L. L. *Phys. Rev. Lett.* **2001**, *86*, 4656−4659.
(9) Choi, H. J.; Roundy, D.; Sun, H.; Cohen, M. L.; Louie, S. G. *Nature* **2002**, *418*, 758−760.
(10) Mishonov, T. M.; Penev, E. S. *Theory of High Temperature Superconductivity: A Conventional Approach*; World Scientific: Singapore, 2011.
(11) Baroni, S.; de Gironcoli, S.; Dal Corso, A.; Giannozzi, P. *Rev. Mod. Phys.* **2001**, *73*, 515−562.
(12) Evans, M. H.; Joannopoulos, J. D.; Pantelides, S. T. *Phys. Rev. B: Condens. Matter Mater. Phys.* **2005**, *72*, 045434.
(13) Kunstmann, J.; Quandt, A. *Phys. Rev. B: Condens. Matter Mater. Phys.* **2006**, *74*, 035413.
(14) Savini, G.; Ferrari, A. C.; Giustino, F. *Phys. Rev. Lett.* **2010**, *105*, 037002.
(15) Profeta, G.; Calandra, M.; Mauri, F. *Nat. Phys.* **2012**, *8*, 131−134.
(16) Ludbrook, B. M.; Levy, G.; Nigge, P.; Zonno, M.; Schneider, M.; Dvorak, D. J.; Veenstra, C. N.; Zhdanovich, S.; Wong, D.; Dosanjh, P.; Straßer, C.; Stöhr, A.; Forti, S.; Ast, C. R.; Starke, U.; Damascelli, A. *Proc. Natl. Acad. Sci. U. S. A.* **2015**, *112*, 11795−11799.
(17) Dai, J.; Li, Z.; Yang, J.; Hou, J. *Nanoscale* **2012**, *4*, 3032−3035.
(18) Shao, D. F.; Lu, W. J.; Lv, H. Y.; Sun, Y. P. *Europhys. Lett.* **2014**, *108*, 67004.
(19) Tang, H.; Ismail-Beigi, S. *Phys. Rev. Lett.* **2007**, *99*, 115501.
(20) Tang, H.; Ismail-Beigi, S. *Phys. Rev. B: Condens. Matter Mater. Phys.* **2009**, *80*, 134113.
(21) Wu, X.; Dai, J.; Zhao, Y.; Zhuo, Z.; Yang, J.; Zeng, X. C. *ACS Nano* **2012**, *6*, 7443−7453.
(22) Bardeen, J.; Cooper, L. N.; Schrieffer, J. R. *Phys. Rev.* **1957**, *108*, 1175−1204.
(23) Migdal, A. B. *Sov. Phys. JETP* **1958**, *7*, 996−1001.
(24) Eliashberg, G. M. *Sov. Phys. JETP* **1960**, *11*, 696−702.
(25) McMillan, W. L. *Phys. Rev.* **1968**, *167*, 331−344.
(26) Allen, P. B.; Dynes, R. C. *Phys. Rev. B* **1975**, *12*, 905−922.
(27) Allen, P. B.; Mitrović, B. *Solid State Physics*; Seitz, F., Turnbull, D., Ehrenreich, H., Eds.; Academic Press: New York, 1982; Vol. *37*, pp 1−92.
(28) Marsiglio, F.; Carbotte, J. P. *Superconductivity*; Bennemann, K. H., Ketterson, J. B., Eds.; Springer: Berlin, 2008; Vol. *1*, pp 73−162.
(29) Giannozzi, P.; Baroni, S.; Bonini, N.; Calandra, M.; Car, R.; Cavazzoni, C.; Ceresoli, D.; Chiarotti, G. L.; Cococcioni, M.; Dabo, I.; Dal Corso, A.; de Gironcoli, S.; Fabris, S.; Fratesi, G.; Gebauer, R.; Gerstmann, U.; Gougoussis, C.; Kokalj, A.; Lazzeri, M.; Martin-Samos, L.; Marzari, N.; Mauri, F.; Mazzarello, R.; Paolini, S.; Pasquarello, A.; Paulatto, L.; Sbraccia, C.; Scandolo, S.; Sclauzero, G.; Seitsonen, A. P.; Smogunov, A.; Umari, P.; Wentzcovitch, R. M. *J. Phys.: Condens. Matter* **2009**, *21*, 395502.
(30) Kohn, W. *Phys. Rev. Lett.* **1959**, *2*, 393−394.
(31) Liu, A. Y.; Mazin, I. I.; Kortus, J. *Phys. Rev. Lett.* **2001**, *87*, 087005.
(32) Nelson, D.; Piran, T.; Weinberg, S. *Statistical Mechanics of Membranes and Surfaces*; World Scientific: Singapore, 2004.
(33) Castro Neto, A. H.; Guinea, F.; Peres, N. M. R.; Novoselov, K. S.; Geim, A. K. *Rev. Mod. Phys.* **2009**, *81*, 109−162.
(34) Feng, B.; Zhang, J.; Zhong, Q.; Li, W.; Li, S.; Li, H.; Cheng, P.; Meng, S.; Chen, L.; Wu, K. *arXiv preprint arXiv:1512.05029* **2015**.
(35) Feng, B.; Zhang, J.; Liu, R.-Y.; Takushi, I.; Lian, C.; Chen, L.; Wu, K.; Li, H.; Meng, S.; Komori, F.; Matsuda, I. *arXiv preprint arXiv:1512.05270* **2015**.
(36) Mannix, A. J.; Zhou, X.-F.; Kiraly, B.; Wood, J. D.; Alducin, D.; Myers, B. D.; Liu, X.; Fisher, B. L.; Santiago, U.; Guest, J. R.; Yacaman, M. J.; Ponce, A.; Oganov, A. R.; Hersam, M. C.; Guisinger, N. P. *Science* **2015**, *350*, 1513−1516.
(37) Zhao, Y.; Zeng, S.; Ni, J. *Phys. Rev. B: Condens. Matter Mater. Phys.* **2016**, *93*, 014502.
(38) Eremets, M. I.; Struzhkin, V. V.; Mao, H.-k.; Hemley, R. J. *Science* **2001**, *293*, 272−274.

DOI: 10.1021/acs.nanolett.6b00070
Nano Lett. 2016, 16, 2522−2526